Original Article

Ultrashort echo time pulse sequences for visualization of deep peripheral fasciae and epimysium in porcine models with histologic correlations

Kun Hwang[1,2#^], Jang Gyu Cha[3#^], Hun Kim[4^], Hyungseok Jang[5^], Dae Joong Kim[6^], Seunghun Lee[7^], Yeo Ju Kim[7^]

[1]Department of Plastic Surgery, Armed Forces Capital Hospital, Seongnam-City, Republic of Korea; [2]Ewha Medical Academy, Ewha Womans University Medical Center, Seoul, Republic of Korea; [3]Department of Radiology, Soonchunhyang University Bucheon Hospital, Bucheon-Si, Republic of Korea; [4]Division of Trauma Surgery, Department of Surgery, Seoul National University Hospital, Seoul, Republic of Korea; [5]Department of Radiology, University of California, San Diego, San Diego, CA, USA; [6]Department of Anatomy, College of Medicine, Inha University, Incheon, Republic of Korea; [7]Department of Radiology, College of Medicine, Hanyang University, Seoul, Republic of Korea

Contributions: (I) Conception and design: YJ Kim, JG Cha, K Hwang; (II) Administrative support: DJ Kim, K Hwang, H Kim; (III) Provision of study materials or patients: JG Cha, DJ Kim, K Hwang, H Kim; (IV) Collection and assembly of data: YJ Kim, JG Cha; (V) Data analysis and interpretation: YJ Kim, JG Cha, DJ Kim, K Hwang, S Lee, H Jang; (VI) Manuscript writing: All authors; (VII) Final approval of manuscript: All authors.

[#]These authors contributed equally to this work and should be considered as co-first authors.

Correspondence to: Yeo Ju Kim, MD, PhD. Department of Radiology, College of Medicine, Hanyang University, 222, Wangsimni-ro, Seongdong-gu, Seoul 04763, Republic of Korea. Email: kimyeoju@hanyang.ac.kr.

Background: The deep peripheral fascia and epimysium are vital for muscle and tendon support, but their tight proton composition results in hypointense signals in conventional spin echo sequences. Ultrashort echo time (UTE) magnetic resonance imaging (MRI), using microsecond TE values, may visualize these structures. The purpose of this study was to evaluate whether UTE pulse sequence with a three-dimensional cone trajectory (3D UTE), with or without fat suppression (FS), can be used to visualize the fascia and epimysium using porcine lower legs as an example.

Methods: The anterior soft tissues of porcine lower legs were dissected and partially separated into distinct layers to expose the deep peripheral fascia, epimysium, and muscle. Axial 3D UTE and 3D UTE FS imaging using dual-echo acquisition and echo subtraction were performed both before and after dissection. Prior to dissection, the thickness, signal-to-noise ratios (SNRs), and contrast-to-noise ratios (CNRs) of structures believed to be deep peripheral fascia and epimysium were measured in both 3D UTE and 3D UTE FS. Post-dissection images were also analyzed to measure the SNRs and CNRs for the deep peripheral fascia and epimysium. Histological evaluations were carried out to verify the identities of the deep peripheral fascia and epimysium, as well as their thickness, and these measurements were compared to imaging findings.

Results: In pre-dissection images obtained with 3D UTE and 3D UTE FS, both the deep peripheral fascia and epimysium exhibited high signal intensity. In the subtraction images, the mean thickness of the deep fascia was 0.87 mm, and that of the epimysium was 0.80 mm when imaged with 3D UTE. This is compared to measurements of 0.77 and 0.22 mm in 3D UTE FS, respectively. Histological analyses confirmed the thickness of the deep peripheral fascia and epimysium as 0.65 and 0.14 mm, respectively. In the post-dissection images, the deep fascia continued to display high signal intensity when compared with adjacent

^ ORCID: Kun Hwang, 0000-0002-1994-2538; Jang Gyu Cha, 0000-0002-3803-4850; Hun Kim, 0000-0002-6296-9584; Hyungseok Jang, 0000-0002-3597-9525; Dae Joong Kim, 0000-0002-7841-4153; Seunghun Lee, 0000-0002-4348-7993; Yeo Ju Kim, 0000-0002-1783-8876.

soft tissues, consistent with the histological findings. Meanwhile, the epimysium showed very low CNRs.

Conclusions: 3D UTE and 3D UTE FS can be used to visualize the deep peripheral fascia with high signal intensity and contrast but are insufficient to show signal intensity in the epimysium.

Keywords: Ultrashort echo time (UTE); deep peripheral fascia; epimysium

Submitted May 17, 2023. Accepted for publication Sep 18, 2023. Published online Oct 11, 2023.
doi: 10.21037/qims-23-687
View this article at: https://dx.doi.org/10.21037/qims-23-687

Introduction

Fascia is made up of sheets of connective tissue that is found below the skin (1). These tissues attach, stabilize, impart strength, maintain vessel patency, separate muscles, and enclose different organs (1). In the limbs, the fascia was divided into superficial fascia, which is a layer of connective tissue located immediately deep to the dermis, and deep fascia, which surrounds muscles (1,2). There are two subtypes of deep fascia such as deep peripheral fascia and epimysium (1,2). The deep peripheral fascia (aponeurotic fascia) is a layer of dense connective tissue arranged in sheets that forms the stocking around the muscles and tendons beneath the subcutaneous layer and lies in continuous contact with the epimysium of the limb (3). The deep peripheral fascia which thins into a tendon and becomes a point of origin or insertion for other muscles is called aponeurosis. The epimysium (epimysial fascia) is a loose connective tissue that consists of collagen fibers and envelopes each muscle (4). Deep peripheral fascia and epimysium protect structures and serve as barriers to tumors or infections in the limb (5,6). However, these fasciae are mainly composed of tissues with tightly bound protons so the signals from these protons decay very quickly. This rapid signal decay results in a hypointense signal when conventional magnetic resonance imaging (MRI) sequences are used (7). Ultrashort echo time (UTE) is an MRI technique that uses even shorter TE values on the order of microseconds (μs) (7). These dramatically shortened TEs allow the depiction of short T2 components as hyperintense signals on UTE imaging (7). UTE has been successfully applied to disk-bone specimens, osteochondral junctions, ligament, tendon and cortical bone in high-resolution imaging to visualize tissue primarily composed of short T2 components (8-12). With three-dimensional (3D) cone trajectory UTE, which is one of several available UTE techniques, short signals can be detected that are less affected by the eddy current effect, and the acquisition time can be reduced by using an efficient 3D spiral pattern, compared to two-dimensional (2D) UTE imaging (13,14). However, there has been no prior study on whether 3D UTE can depict the deep peripheral fascia and epimysium in a manner that directly correlates with histology. Therefore, the purpose of our study was to evaluate whether UTE with three-dimensional cone trajectory (3D UTE), with or without fat suppression (FS), can visualize the fascia and epimysium, using porcine legs as an example.

Methods

The present study comprised two sets of experiments, ethical approval was exempted by the Institutional Review Board of Inha University Hospital due to the use of cadaveric animal specimen. In Experiment No. 1, the thickness, signal-to-noise ratio (SNR) and contrast-to-noise ratio (CNR) of structures thought to be deep peripheral fascia and epimysium were measured in 3D UTE and 3D UTE with fat suppression (3D UTE FS) in three porcine lower legs. In Experiment No. 2, three porcine lower legs were dissected and subjected to 3D UTE and 3D UTE FS. These processes were undertaken for histologic verification of the deep peripheral fascia and epimysium, as well as for the exclusion of any artifacts within the tissue boundaries that could mimic these structures.

Experiment No. 1

MRI protocol

Three fresh porcine lower legs (two right lower legs and one left lower leg) from the tibial plateau to the tibial plafond from animals sacrificed for meat in the slaughterhouse were obtained within 24 hours of death. No live animals were used in this study and were sacrificed for the study. All three porcine lower legs underwent MRI using 3T MR scanners (Discovery 750 W, GE Healthcare, Waukesha,

Table 1 MRI protocol

Sequence parameters	Porcine lower leg				
	3D UTE		3D UTE FS		T1WI
	Echo-1	Echo-2	Echo-1	Echo-2	
TR (ms)	11.4		22		793
TE (ms)	0.032	4.4	0.032	4.4	7.66
FA (°)	17		17		111
BW (kHz)	62.5		62.5		62.5
ETL	NA		NA		3
NEX	NA		NA		1
Matrix size	300×300		300×300		300×300
Voxel size (mm^3)	0.5×0.5×3				NA
Number of projections	20,217		20,217		NA
ST/gap (mm)	3/0				
FOV (x, y, z axis, mm)	150×150×90				150×150
Scan time (min:s)	3:14		6:14		3:30

The frequency encoding direction of T1WI is anteroposterior. MRI, magnetic resonance imaging; 3D UTE, ultrashort echo time pulse sequence with three-dimensional cone trajectory; 3D UTE FS, ultrashort echo time pulse sequence with three-dimensional cone trajectory with chemical shift-based fat saturation fat suppression; T1WI, T1 weighted fast spin echo sequence; Echo-1, the 1st echo image; Echo-2, the 2nd echo image; TR, repetition time; TE, echo time; FA, flip angle; BW, bandwidth; ETL, echo train length; NEX, number of excitation; ST, section thickness; FOV, field of view.

WI, USA), with a maximum peak gradient amplitude of 44 mT/m and a slew rate of 200 T/m/s in conjunction with a 16-channel receive-only phrase array coil (Gem flex large, GE Healthcare). Axial T1 weighted fast spin echo sequence (T1WI), 3D UTE, and 3D UTE FS were performed (*Table 1*). The 3D UTE sequence utilized a short nonselective hard pulse (duration =100 μs) for volumetric excitation, followed by dual-echo 3D cone acquisition with a minimal nominal TE of 32 μs (15,16) (*Figure 1*). The first free induction decay UTE acquisition with a minimal nominal TE of 32 μs detected signals from both long- and short-T2 components, whereas the second gradient recalled echo with a TE of 4.4 ms detected signals from longer-T2 components. Subtraction of the second echo from the first suppresses signals from the longer-T2 components and typically provides high contrast for tissues whose T2* lies between the two TEs.

FS was carried out using the conventional chemical shift-based fat saturation (CHESS). With chemical shift-based fat saturation, a spectrally selective radiofrequency (RF) pulse is followed by a gradient spoiler. The saturation pulse [minimum-phase Shinnar-Le Roux (mip-SLR) design with a duration of 8 ms and bandwidth of 500 Hz] was centered on the fat peak with a flip angle of no less than 90°, followed by a gradient spoiler to crush all the excited transverse magnetizations. Short hard pulses are then used to excite the signal. The scan times were 3 min 30 s for T1WI, 3 min 14 s for 3D UTE, and 6 min 14 s for 3D UTE FS (*Table 1*).

Image analysis

To ensure accurate image analysis, the terminology for the components of the fascial system was defined as follows. The deep peripheral fascia was defined as a low signal intensity structure on T1WI and located deep to the subcutaneous fat and superficial to muscle (2). The epimysium was a structure that surrounds each muscle but it is usually not visible in T1WI (2). Chemical shift artifact generates a low signal intensity which surrounds muscle in the frequency encoding direction (2). *Figure 2* showed a schematic diagram of the fascial system with a detailed description.

Referring to the above definitions and T1WI, the structures at the locations of the deep peripheral fascia and epimysium were searched in the 3D UTE, and 3D UTE FS for all three porcine lower legs by two musculoskeletal

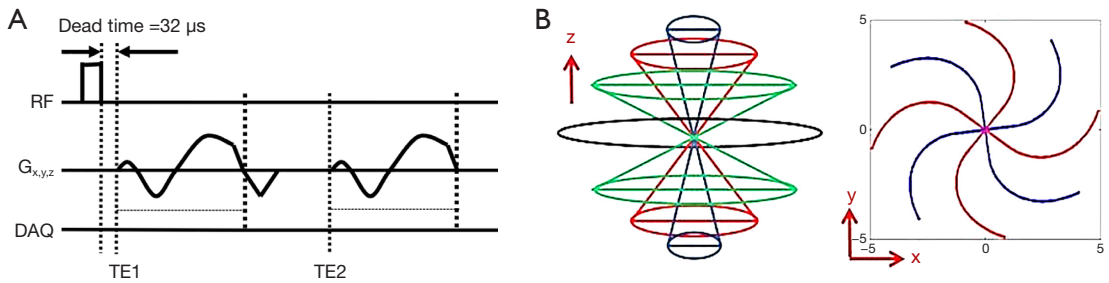

Figure 1 Sequence diagram of 3D UTE. (A) In the basic 3D UTE, a short rectangular pulse was used for signal excitation followed by 3D spiral sampling with a minimal nominal TE (TE1) of 32 μs. The TE2 is 4.4 ms in this study. (B) The spiral trajectories are arranged with conical view ordering. RF, radiofrequency pulse; DAQ, data acquisition; TE, echo time; TE1, first TE; TE2, second TE; 3D UTE, ultrashort echo time pulse sequence with three-dimensional cone trajectory.

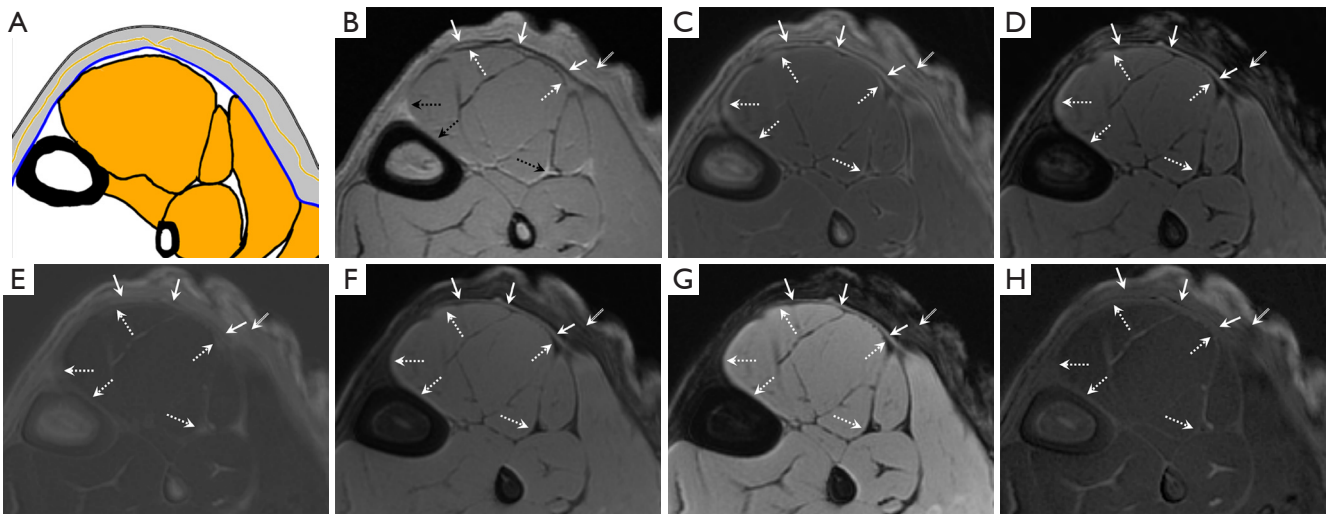

Figure 2 Schematic drawing of an axial image of porcine lower leg illustrating its fascial anatomy and corresponding images of MRI. (A) Schematic drawing of an axial image of porcine lower leg. The superficial fascia (gray area) is a three-dimensional connective tissue network in the hypodermis that contains fibrous tracts (yellow line, membranous superficial fascia), fat lobules, and superficial nerves and vessels. The deep peripheral fascia (blue line) is located deep to the hypodermis and superficial to the muscle. The membranous superficial fascia (yellow line) and deep peripheral fascia are histologically identical except for their location but usually, the deep peripheral fascia is slightly thicker than the membranous superficial fascia. In some areas, the deep fascia and membranous superficial fascia are contiguous. The epimysium (black lines around the orange area) was a structure that surrounds each muscle (orange areas). (B) Axial T1WI shows the deep peripheral fascia (solid white arrows) as a low signal intensity structure that is located deep to the subcutaneous fat and superficial to muscle compartment. The epimysium was a structure that surrounds each indivisual muscle but it is usually not visible (black dashed arrows) in T1WI. Chemical shift artifact (white dashed arrows) generates a low signal intensity which surrounds muscle in the frequency encoding direction but should not be confused with epimysium. Note multilayers of the thin membranous superficial fascia (double line arrow). (C-H) Corresponding images of 3D UTE with the 1st echo (C), the 2nd echo (D), and the subtraction (E) and 3D UTE FS with the 1st echo (F), the 2nd echo (G), and the subtraction (H). White arrows indicate the area of expected deep peripheral fascia. White dashed arrows are the area of expected epimysium, white double line arrow is the membranous superficial fascia. MRI, magnetic resonance imaging; 3D UTE, ultrashort echo time pulse sequence with three-dimensional cone trajectory; 3D UTE FS, ultrashort echo time pulse sequence with three-dimensional cone trajectory with chemical shift-based fat saturation fat suppression.

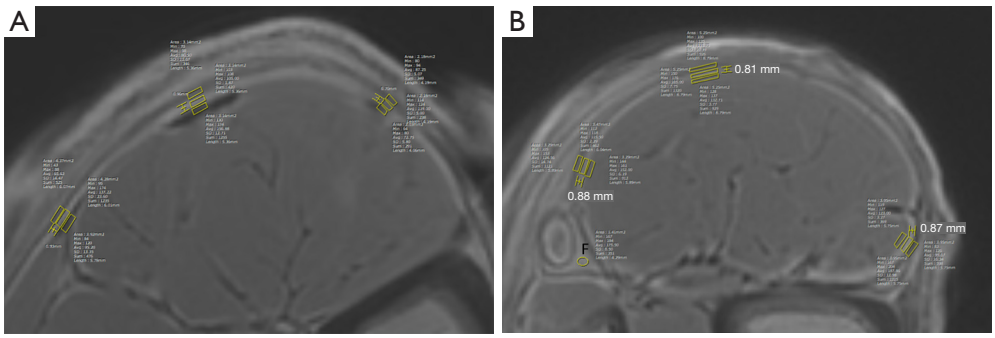

Figure 3 Example images of measurement of thickness and SNRs of deep peripheral fascia (A) and epimysium (B) in the 1st echo image of 3D UTE of the porcine lower leg. Three areas—the right lateral, central, and left lateral areas—where the deep peripheral fascia and adjacent muscle are separated by fat, were chosen for measuring the deep peripheral fascia within axial image (A). For the evaluation of the epimysium, another image was selected, one that displayed a well-visualized muscle surface. Measurements were taken at the anterior, right lateral, and left lateral surfaces of the muscle (B). The evaluation of thickness involved measuring the width of high signal intensity in areas believed to be either deep peripheral fascia or epimysium. For SNR measurements, variable-sized ROIs were drawn around the high signal intensity, believed to be either deep fascia or epimysium, as well as the adjacent soft tissue and intermuscular fat (F), using a free-hand technique. SNRs, signal-to-noise ratios; 3D UTE, ultrashort echo time pulse sequence with three-dimensional cone trajectory; ROIs, regions of interest.

radiologists with consensus. For quantitative analysis, the thickness and SNR were measured in the 1st echo, 2nd echo, and subtraction images of 3D UTE and 3D UTE FS for each porcine lower leg using a PACS system (Infinitt G7, Infinitt Healthcare, Seoul, Republic of Korea) by two musculoskeletal radiologists independently. Images were displayed one by one on the PACS monitor and then magnified ten times. In terms of deep peripheral fascia, three areas (right lateral, central, and left lateral area) where deep peripheral fascia and adjacent muscle were separated by fat were selected for the measurement (*Figure 3*). For epimysium, the anterior, right lateral, and left lateral surface of the muscle where epimysium and deep peripheral fascia were separated by fat were selected (*Figure 3*). For SNR measurements, region of interests (ROIs) of varying sizes were drawn using a freehand technique on areas of high signal intensity, believed to be deep peripheral fascia or epimysium, and adjacent soft tissue. A circular ROI was drawn on the intermuscular fat. To estimate the standard deviation (SD), a circular ROI with a size of 69.89 mm^2 was positioned in the background noise. The SNRs for the deep peripheral fascia, epimysium, adjacent soft tissue, and intermuscular fat were calculated by dividing the signal level by the SD of the noise. CNRs between the deep peripheral fascia or epimysium and adjacent tissue were obtained by taking the absolute value of the difference in the SNR between the deep peripheral fascia or epimysium and adjacent tissue.

For the evaluation of thickness, the width of high signal intensity in areas considered to be deep peripheral fascia or epimysium was measured at a location adjacent to where we measured SNR. All measurement for the SNR and the thickness was done in the 1st echo image of 3D UTE (FS) and copied to the 2nd echo and subtraction image.

Experiment No. 2

Tissue preparation and MRI scan

Following Experiment No. 1, the three porcine lower legs were stored in a refrigerator at 4 ℃ for one day. Experiment No. 2 was conducted the subsequent day after the samples were left at room temperature for one hour. The anterior extensor compartment of each porcine lower leg, located distally to the tibial tuberosity, along with the overlying soft tissue, was divided into three zones. These zones were then partially peeled off in layers by a plastic surgeon as follows: from the skin to the subcutaneous layer just over the deep peripheral fascia (zone 1, *Figure 4A*), from the skin to the deep peripheral fascia (zone 2, *Figure 4B*), and from the skin to the middle portion of the muscle belly (zone 3, *Figure 4C*). The size of each zone was 2.5×3 cm^2 (transverse × longitudinal). One side of each peeled-off tissue (flap) was attached and was therefore continuous with adjacent normal tissue. Ultrasound transmission gel (Aquasonic clear gel,

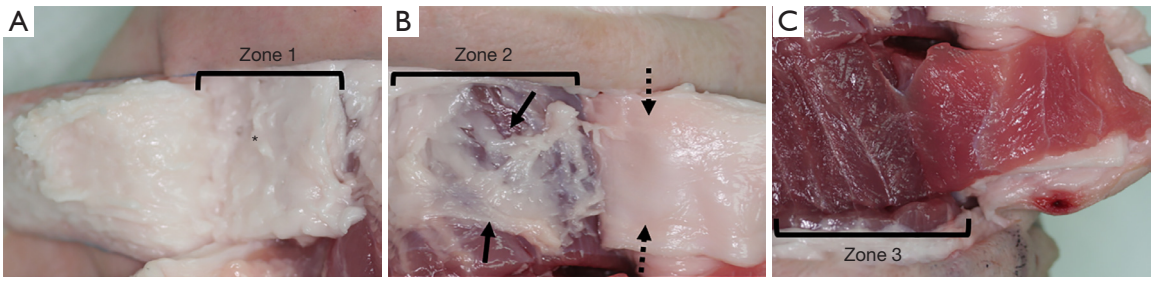

Figure 4 Photograph of the dissected anterior compartment of a fresh porcine lower leg. Three different partially peeled tissues were prepared. Zone 1 (A) was dissected from the skin into the subcutaneous layer for exposure of deep peripheral fascia. Some subcutaneous fat remains over the deep peripheral fascia (asterisk). Zone 2 (B) was dissected from the skin into the deep peripheral fascia for exposure of epimysium (arrows). Note the smooth thick fibrous deep peripheral fascia (dashed arrows) on the flap. Zone 3 (C) was dissected from the skin to the superficial portion of the muscle bellies for the removal of epimysium. One side of each peeled-off tissue was left attached, and was therefore continuous with the adjacent normal tissue.

Parker Laboratories Inc., NJ, USA) was applied between flaps and resection beds. MRI scans were performed using the same protocol as the Experiment No. 1.

Histological evaluation

After the MRI scan, the flaps and remaining tissues from all zones were resected, fixed in 4% neutral buffered formalin, and embedded in paraffin blocks. Standard histologic procedures were applied to these paraffin-embedded tissue blocks, which were sectioned axially at a 10 μm slice thickness, with 6 mm intervals. As a result, four slices were collected from each zone throughout the block. All samples were then stained with Masson's trichrome stain and observed under a light microscope. A histologist evaluated the slides for the presence of deep peripheral fascia and epimysium across all. The thickness of deep peripheral fascia and epimysium were also measured by magnifying the slide image 4 times and designated three areas where the deep peripheral fascia and epimysium were well separated from each other and distinguished from the surrounding tissue. All measurement of thickness was done using ImageJ software (National Institutes of Health, Bethesda, MD, USA).

Imaging analysis with histologic correlation

Two radiologists assessed the presence of sheet-like structures in remaining tissue correlating with histology. SNRs and CNRs were measured by two musculoskeletal radiologists independently in the same way as in Experiment No. 1. ROIs at expected deep peripheral fascia or epimysium sites and adjacent soft tissue as with Experiment No. 1. CNRs was calculated by subtracting SNR of deep peripheral fascia or epimysium from SNR of adjacent soft tissue.

Statistical analysis

Descriptive analysis was done for all quantitative measurement of image analysis and histologic evaluation. All quantitative measures taken in the imaging analysis of Experiment No. 1 and No. 2 by two musculoskeletal radiologists were subjected to an interobserver agreement using the interclass coefficient. The strength of the interobserver agreement indicated with κ values was classified as follows: poor, κ<0.0; slight, κ=0.0–0.20; fair, κ=0.21–0.40; moderate, κ=0.41–0.60; substantial, κ=0.61–0.80; and almost perfect, κ=0.81–1.00 (17).

Results

Experiment No. 1

Table 2 shows the mean SNRs, CNRs, and mean thickness of deep peripheral fascia and epimysium in 3D UTE and 3D UTE FS by two radiologists. All measurements showed excellent agreement with κ values above 0.8. Deep peripheral fascia and epimysium displayed high signal intensity, while epimysium had a lower SNR. In 3D UTE, pixels with lower signal intensity than intermuscular fat were seen around the deep peripheral fascia and epimysium. Deep peripheral fascia showed higher SNR and CNR in 3D UTE than in 3D UTE FS. Generally, the subtraction images showed low SNR and CNR. In terms of thicknesses, deep peripheral fascia, and epimysium were thicker

Table 2 Mean SNRs, and CNRs of deep peripheral fascia, epimysium and adjacent soft tissue and mean thickness of deep fascia and epimysium in 3D UTE, and 3D UTE FS in the pre-dissection MRI of three porcine lower legs of Experiment No. 1 and mean thickness of deep peripheral fascia and epimysium in histologic slides in Experiment No. 2

Quantitative variables for each reader	Mean size of ROI (mm^2)	3D UTE			3D UTE FS			κ
		Echo-1	Echo-2	Sub	Echo-1	Echo-2	Sub	
SNR of DF								
R1	3.23	280.48 (67.54)	110.02 (42.62)	68.22 (23.82)	140.26 (73.28)	121.51 (67.9)	30.29 (6.65)	0.85 (P<0.001)
R2	3.40	337.51 (195.58)	143.6 (31.11)	66.09 (22.98)	130.26 (84.05)	91.55 (61.16)	23.38 (8.88)	
SNR of fat superficial to DF								
R1	3.23	168.72 (43.65)	45.76 (34.89)	51.29 (26.00)	76.81 (50.36)	56.34 (40.52)	19.43 (0.93)	0.94 (P<0.001)
R2	3.40	176.50 (41.94)	59.98 (26.30)	58.39 (15.43)	81.00 (46.86)	46.63 (29.33)	18.23 (7.67)	
SNR of fat beneath DF								
R1	3.23	140.54 (56.85)	49.03 (23.38)	30.2 (19.64)	85.2 (49.42)	76.31 (38.32)	15.95 (7.54)	0.81 (P<0.001)
R2	3.40	188.26 (165.42)	61.76 (30.20)	29.53 (10.82)	157.05 (36.81)	53.64 (33.72)	14.95 (7.53)	
SNR of intermuscular fat								
R1	1.41	103.65 (31.02)	47.1 (16.79)	51.31 (7.41)	36.52 (9.96)	14.54 (7.74)	14.22 (2.84)	0.98 (P<0.001)
R2	1.50	113.44 (45.92)	49.00 (22.47)	47.17 (6.55)	45.61 (15.06)	19.59 (3.94)	18.7 (4.72)	
SNR of EP								
R1	3.50	143.34 (46.11)	127.25 (56.59)	39.48 (15.69)	140.57 (67.88)	102.12 (61.12)	19.61 (13.79)	0.98 (P<0.001)
R2	3.40	149.94 (38.93)	136.61 (46.94)	40.3 (23.45)	150.88 (68.88)	124.84 (60.11)	23.66 (19.21)	
SNR of fat superficial to EP								
R1	3.50	87.22 (26.59)	55.48 (30.89)	39.81 (13.06)	68.15 (36.85)	45.43 (35.19)	21.81 (12.68)	0.93 (P<0.001)
R2	3.40	95.40 (18.00)	52.70 (20.37)	37.97 (15.39)	69.52 (38.18)	41.37 (27.58)	20.25 (10.9)	
SNR of the adjacent muscle beneath the EP								
R1	3.50	100.50 (27.37)	100.27 (37.69)	20.54 (12.74)	118.59 (48.03)	91.03 (54.34)	15.23 (13.46)	0.99 (P<0.001)
R2	3.40	105.98 (27.02)	103.87 (33.40)	17.97 (9.04)	126.70 (51.33)	105.25 (46.62)	15.60 (11.85)	
CNR between DF and fat superficial to DF	–							
R1		111.76 (64.89)	64.25 (19.22)	18.05 (14.83)	63.45 (28.86)	65.17 (39.72)	10.86 (6.48)	0.87 (P<0.001)
R2		163.69 (180.08)	83.61 (30.32)	19.48 (19.74)	55.61 (34.16)	46.87 (32.70)	7.18 (4.40)	

Table 2 (*continued*)

Table 2 (*continued*)

Quantitative variables for each reader	Mean size of ROI (mm^2)	3D UTE			3D UTE FS			κ
		Echo-1	Echo-2	Sub	Echo-1	Echo-2	Sub	
CNR between DF and fat beneath DF	–							
R1		139.95 (31.74)	60.99 (28.67)	38.02 (15.19)	55.06 (27.42)	45.2 (36.92)	14.34 (4.75)	0.86 (P<0.001)
R2		201.27 (174.14)	81.83 (32.13)	36.56 (18.44)	51.63 (33.07)	49.26 (27.26)	10.93 (7.49)	
CNR between EP and fat superficial to the EP	–							
R1		56.11 (35.03)	71.77 (37.90)	11.7 (11.68)	72.41 (36.63)	56.69 (29.92)	5.21 (4.41)	0.96 (P<0.001)
R2		54.54 (30.48)	77.01 (27.35)	9.1 (7.57)	81.36 (38.39)	83.48 (36.99)	4.96 (9.68)	
CNR between EP and the adjacent muscle beneath EP	–							
R1		42.84 (24.20)	26.97 (25.48)	18.94 (5.42)	21.98 (27.12)	13.22 (16.28)	5.49 (5.23)	0.92 (P<0.001)
R2		43.96 (19.88)	25.85 (17.39)	22.33 (18.24)	24.18 (25.61)	21.26 (27.98)	9.11 (13.90)	
Thickness of DF (mm)	–							
R1		0.93 (0.19)	0.75 (0.14)	0.9 (0.19)	0.72 (0.15)	0.65 (0.2)	0.79 (0.19)	0.97 (P<0.001)
R2		0.93 (0.15)	0.74 (0.11)	0.85 (0.15)	0.70 (0.13)	0.67 (0.24)	0.75 (0.18)	
Histology				0.65 (0.26)				
Thickness of EP (mm)	–							
R1		0.85 (0.22)	0.64 (0.13)	0.81 (0.19)	0.63 (0.17)	0.51 (0.3)	0.24 (0.36)	0.99 (P<0.001)
R2		0.91 (0.28)	0.64 (0.14)	0.8 (0.17)	0.61(0.16)	0.49 (0.3)	0.22 (0.34)	
Histology				0.14 (0.06)				

The number in parentheses is the standard deviation. The number on the histology row is the average value of deep peripheral fascia or epimysium measured on the histologic slides and the parentheses are the standard deviation. SNRs, signal-to-noise ratios; CNRs, contrast-to-noise ratios; 3D UTE, ultrashort echo time pulse sequence with three-dimensional cone trajectory; 3D UTE FS, ultrashort echo time pulse sequence with three-dimensional cone trajectory with chemical shift-based fat saturation fat suppression; MRI, magnetic resonance imaging; ROI, region of interest; Echo-1, the 1st echo image; Echo-2, the 2nd echo image; Sub, subtraction image from the 1st echo to 2nd echo image; DF, deep peripheral fascia; R1, reader 1; R2, reader 2; EP, epimysium.

in 3D UTE than that in 3D UTE FS. The thickness difference between 3D UTE and 3D UTE FS was larger in epimysium than in deep peripheral fascia. For example, in the subtraction image, the mean thickness of the deep peripheral fascia, as measured by both reviewers, was 0.87 in 3D UTE and 0.77 in 3D UTE FS. In contrast, the mean thickness of the epimysium was 0.80 and 0.22, respectively.

Experiment No. 2

In histology, the mean thickness of deep peripheral fascia was 0.65 mm, while that of epimysium was 0.14 mm (*Table 2*). The average SNR and CNR of the expected site of deep peripheral fascia and epimysium at the remaining tissue of post-dissection MRI of the three porcine lower legs were shown in *Table 3*. All measurements showed substantial to excellent agreement with κ values above 0.7.

- Zone 1 (*Figure 5*): histologically, the deep peripheral fascia and epimysium were observed in the remaining tissue in all three specimens (*Figure 5A*). Deep peripheral fascia showed a low signal on T1WI, and high signal on 3D UTE and 3D UTE FS in all three specimens (*Figure 5C-5I*). The 1st echo image of 3D UTE showed the highest SNR and CNR. The subtraction images showed much lower CNR, especially for that of 3D UTE FS (*Table 3*).
- Zone 2 (*Figure 5*): histology showed deep peripheral fascia at the flap and a very thin epimysium along the surface of the remaining tissue in all three specimens (*Figure 5B*). T1WI revealed a minimal amount of fat and low signal intensity of chemical shift artifact at the expected site of epimysium. 3D UTE and 3D UTE FS showed high signal intensity at the expected site of epimysium but the CNR is much lower than the deep peripheral fascia, especially for 3D UTE FS (*Figure 5C-5I*, *Table 3*).
- Zone 3 (*Figure 6*): histology revealed only the muscles of the flap (*Figure 6A*). MRI showed no definite sheet-like structure along the surface of the remaining tissue in all sequences of the three specimens with a very low CNR of the resected muscle surface (*Figure 6B-6H*, *Table 3*).

Discussion

Our study found that 3D UTE and UTE FS depicted deep peripheral fascia but failed to show meaningful signal and contrast for epimysium. Anatomical studies show that deep peripheral fascia, consisting of dense connective tissue with inelastic collagen fibers, is easily separable from underlying limb muscles (3,4,6). Due to its short T2 value, deep peripheral fascia has low signal intensity in clinical T1- and T2-weighted images (7). In our study, 3D UTE and 3D UTE FS showed bright contrast for deep peripheral fascia, correlating with histological findings. However, differences in appearance between 3D UTE and 3D UTE FS were observed. First, low signal intensities around the high signal of deep peripheral fascia were seen, which was more prominent in 3D UTE than that of 3D UTE FS, representing the effect of chemical shift artifact (7,18,19). A chemical shift has been known to appear in the frequency direction, which displaces the pixel location of the fat signal in conventional Cartesian MR sequences, but can take the form of signal cancellation or blurring near the fat-water boundaries in a non-Cartesian radial or cone trajectory sequence, similar to the 3D UTE used in this study (19). This effect disappears with FS (7,18). Second, the high signal intensity appeared thicker in 3D UTE than in 3D UTE FS. The chemical shift artifact overlapping with the deep peripheral fascia's high signal intensity may cause it to appear thicker and more intense in 3D UTE than in 3D UTE FS. Another explanation for the thickness difference is that fat saturation pulses partially saturate short T2 tissues' signals, causing signal attenuation, while not affecting long T2 tissues in conventional imaging (20,21). Furthermore, a relatively large saturation flip angle (i.e., no less than 90°) leads to indirect signal attenuation induced by the magnetization transfer (MT) effects, especially for the collagen-rich tissues (22,23). In our study, 3D UTE FS had much lower SNR and CNR values in the deep peripheral fascia and epimysium than 3D UTE, which may reflect the signal attenuation effect on these short T2 tissues.

In our porcine model, the epimysium was a thin, loose connective tissue. In Experiment No. 1, muscle surfaces, expected site of epimysium, also show high signal intensity in 3D UTE, but appear to be affected by chemical shift artifacts for the same reasons as deep peripheral fascia. Mean epimysium thickness was only 0.14 mm in histology which is difficult to measure, but in the 3D UTE, it was measured to be much thicker than the actual size. Furthermore, the mean thickness of epimysium showed much difference between 3D UTE and 3D UTE FS than that of deep peripheral fascia. In Experiment No. 2, CNR at the expected site of epimysium is generally low. From these results, it is considered that the signal related to the chemical shift artifact has a greater effect than the actual

Table 3 The average SNR and CNR of the expected site of deep peripheral fascia and epimysium at the remaining tissue of post-dissection MRI of the three porcine lower legs

Zone	Quantitative variables for each reader	Mean size of ROI (mm^2)	3D UTE			3D UTE FS			κ
			Echo-1	Echo-2	Sub	Echo-1	Echo-2	Sub	
1	SNR of DF								
	- R1	11.00	137.86 (101.82)	87.82 (27.48)	36.26 (3.02)	102.76 (77.82)	92.90 (49.38)	21.25 (4.04)	0.85 (P<0.001)
	- R2	10.00	125.12 (39.90)	63.50 (20.36)	26.29 (7.93)	98.98 (34.86)	64.14 (19.81)	19.47 (4.16)	
	SNR of fat beneath DF								0.90 (P<0.001)
	- R1	11.00	76.83 (62.22)	66.45 (38.17)	22.73 (13.29)	56.20 (17.30)	56.01 (39.10)	15.31 (6.58)	
	- R2	10.00	76.39 (41.35)	48.12 (31.30)	17.14 (7.64)	63.68 (29.03)	56.83 (33.73)	13.39 (3.89)	
	CNR between DF and fat beneath DF								
	- R1	–	61.03 (43.09)	21.36 (11.44)	14.14 (12.80)	46.56 (64.07)	36.88 (45.48)	5.94 (3.10)	0.77 (P=0.002)
	- R2	–	48.72 (9.45)	15.40 (14.41)	9.15 (5.78)	35.30 (40.92)	14.93 (3.74)	6.08 (1.81)	
2	SNR of EP								
	- R1	5.20	84.37 (20.96)	99.94 (68.96)	27.51 (0.14)	98.60 (23.00)	112.78 (56.15)	13.29 (1.40)	0.95 (P<0.001)
	- R2	5.40	116.25 (62.13)	90.96 (63.77)	17.29 (4.94)	116.70 (44.67)	105.42 (45.11)	13.17 (0.64)	
	SNR of the muscle beneath EP								
	- R1	19.25	58.59 (12.19)	74.37 (60.53)	9.16 (3.12)	89.08 (24.45)	105.06 (54.30)	9.73 (1.68)	0.95 (P<0.001)
	- R2	20.00	80.89 (33.17)	65.65 (47.00)	8.43 (3.99)	106.06 (43.93)	96.85 (48.94)	11.62 (3.04)	
	CNR between EP and the muscle beneath EP								
	- R1	–	25.78 (9.65)	25.58 (15.49)	18.35 (3.10)	9.52 (2.85)	7.72 (5.11)	3.57 (2.84)	0.77 (P=0.002)
	- R2	–	35.36 (29.00)	25.31 (20.14)	8.86 (8.13)	10.64 (3.43)	8.58 (6.94)	1.55 (2.60)	
3	SNR of the muscle surface								
	- R1	5.60	109.66 (51.47)	92.47 (27.90)	13.12 (1.85)	140.32 (48.22)	161.32 (114.12)	15.72 (2.98)	0.71 (P=0.007)
	- R2	5.30	70.89 (20.59)	92.52 (34.60)	14.14 (0.37)	294.33 (322.96)	206.20 (185.74)	13.55 (8.87)	
	SNR of the muscle								
	- R1	20.61	112.32 (56.74)	91.21 (29.69)	15.10 (4.38)	138.15 (48.88)	155.37 (110.69)	18.29 (3.62)	0.70 (P=0.008)
	- R2	21.00	75.74 (28.54)	91.55 (35.28)	16.00 (1.49)	293.19 (323.31)	196.17 (174.42)	16.33 (8.82)	
	CNR between the muscle surface and the muscle								
	- R1	–	4.82 (4.64)	2.25 (0.82)	2.62 (1.54)	2.17 (0.84)	5.95 (4.88)	2.57 (2.19)	0.83 (P<0.001)
	- R2	–	5.04 (8.23)	1.99 (0.76)	1.86 (1.14)	1.14 (1.11)	10.03 (11.40)	2.78 (3.91)	

The number in parentheses is the standard deviation. DF: the expecting site of deep peripheral fascia in remaining tissue of zone 1; EP: the expecting site of epimysium in the remaining tissue of zone 2. SNR, signal-to-noise ratio; CNR, contrast-to-noise ratio; MRI, magnetic resonance imaging; ROI, region of interest; 3D UTE, ultrashort echo time pulse sequence with three-dimensional cone trajectory; Echo-1, the 1st echo image; Echo-2, the 2nd echo image; Sub, subtraction image from the 1st echo to 2nd echo image; 3D UTE FS, ultrashort echo time pulse sequence with three-dimensional cone trajectory with chemical shift-based fat saturation fat suppression; DF, deep peripheral fascia; R1, reader 1; R2, reader 2; EP, epimysium.

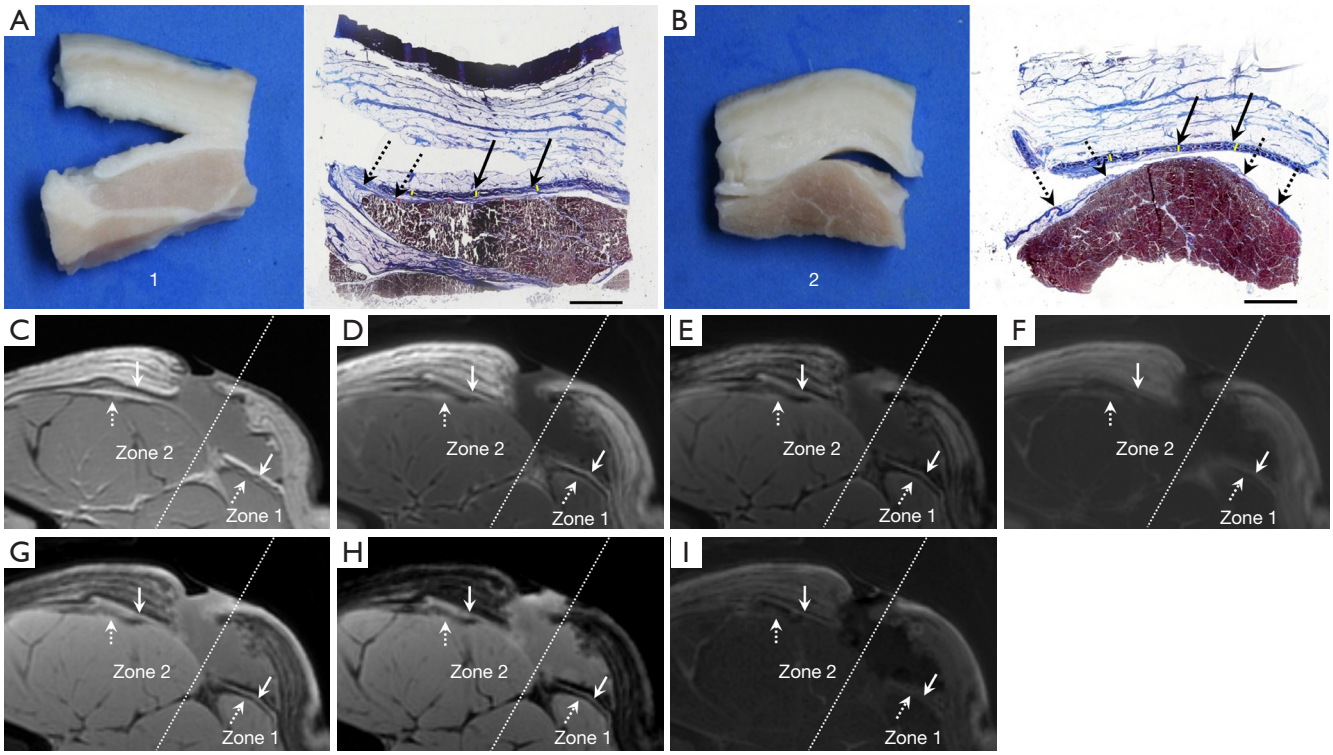

Figure 5 Histologic findings and MRI images of zone 1 and 2 in Experiment No. 2. (A) Gross specimen (left) and histology stained with Masson's trichrome stain (right) of zone 1. Note that the deep peripheral fascia (arrows) and thin, loose epimysium (dashed arrows) were observed in the remaining tissue on histology. The black horizontal bar at the right bottom of histology is a metric scale which is 5 mm. To measure the thickness, three areas were designated where the deep peripheral fascia and epimysium were well separated from each other and distinguished from the surrounding tissue. The yellow lines are exmples of the thickness of the deep fascia and the red lines are those of the epimysium. The actual measurements were made using ImageJ software (National Institutes of Health, Bethesda, MD, USA) which are not shown here. (B) Gross specimen (left) and histology stained with Masson's trichrome stain (right) of zone 2. Histologic findings showed detached deep peripheral fascia (arrows) at the peeled-off tissue and a very thin epimysium (dashed arrows) along the surface of the remaining tissue. Note the metric scale (5 mm) at the right bottom of histology. Again, the yellow lines are exmples of the thickness of the deep fascia and the red lines are those of the epimysium. (C) On T1WI, the low signal intensity of the deep peripheral fascia (arrow in zone 1) and low signal intensity of the chemical shift artifact at the muscle surface (dashed arrow in zone 1) were observed in the remaining tissue of zone 1. In zone 2, the low signal intensity of the deep peripheral fascia (arrow in zone 2) is seen at the flap, and low signal intensity of the chemical shift artifact of muscle surface (dashed arrow in zone 2) is seen in the remaining tissue. (D-F) Axial images of the 1st echo (D), 2nd echo (E), and subtraction (F) of 3D UTE. In zone 1, the deep peripheral fascia (arrow in zone 1) showed high signal intensity in the remaining tissue. In zone 2, the deep peripheral fascia was observed at the flap (arrow in zone 2). The muscle surface (dashed arrow in zone 2) showed high signal intensity but the CNR is much lower than the deep peripheral fascia. Image degradation is seen at the subtraction image. (G-I) Axial images of the 1st echo (G), 2nd echo (H), and subtraction (I) of 3D UTE FS. In zone 1, the deep peripheral fascia (arrow in zone 1) showed high signal intensity in the remaining tissue. In zone 2, the deep peripheral fascia (arrow in zone 2) was observed at the flap. The muscle surface (dashed arrow in zone 2) showed a subtle high signal. The subtraction image shows poor image quality. MRI, magnetic resonance imaging; 3D UTE, ultrashort echo time pulse sequence with three-dimensional cone trajectory; CNR, contrast-to-noise ratio; 3D UTE FS, ultrashort echo time pulse sequence with three-dimensional cone trajectory with chemical shift-based fat saturation fat suppression.

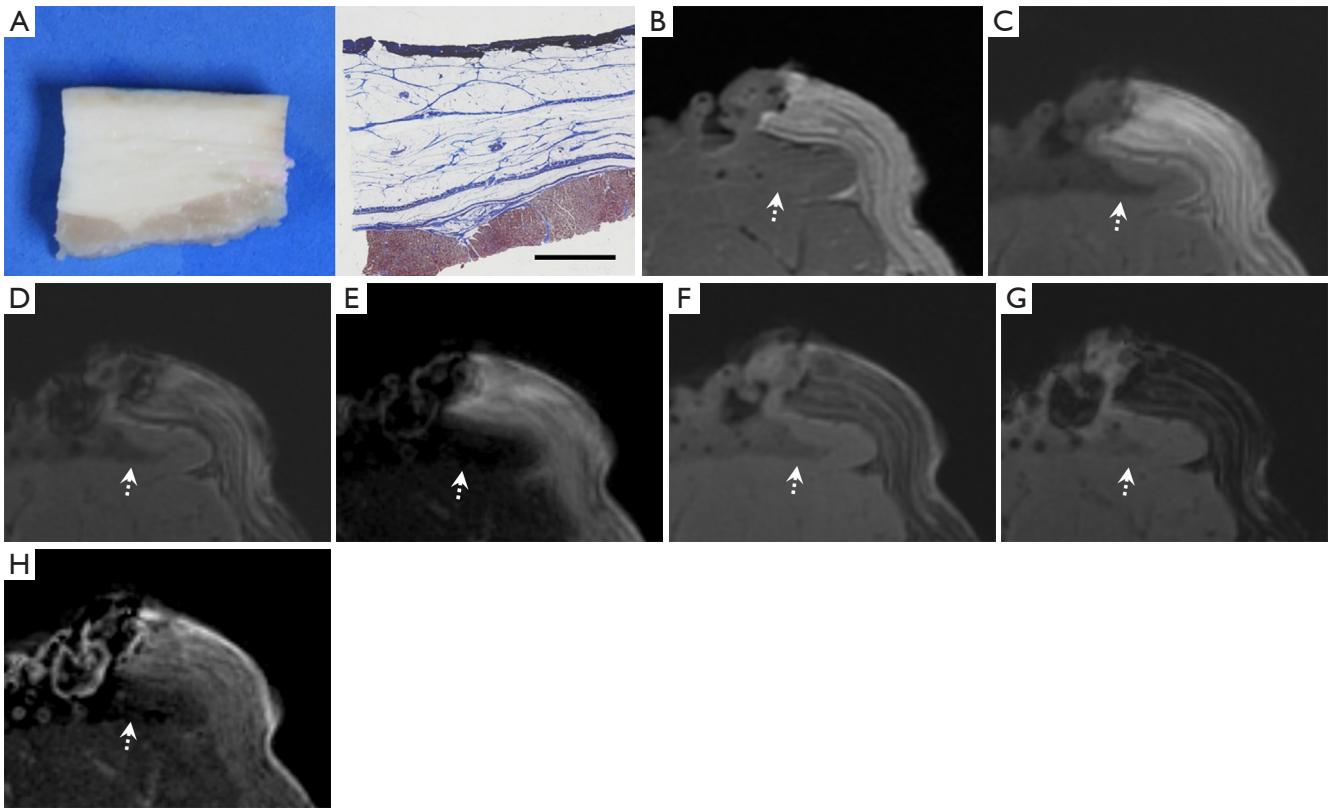

Figure 6 Histologic findings and images of MRI of zone 3 in Experiment No. 2. (A) Gross specimen (left) and histology stained with Masson's trichrome stain (right) of zone 3 showing the detached muscle and overlying subcutaneous layer. Note the metric scale (5 mm) at the right bottom of histology. (B-H) MRI showing no definite signal intensity (dashed arrow) at the surface of the remaining tissue on T1WI (B), 3D UTE (C: the 1st echo, D: the 2nd echo, E: subtraction image), and 3D UTE FS (F: the 1st echo, G: the 2nd echo, H: subtraction image). MRI, magnetic resonance imaging; T1WI, T1 weighted fast spin echo sequence; 3D UTE, ultrashort echo time pulse sequence with three-dimensional cone trajectory; 3D UTE FS, ultrashort echo time pulse sequence with three-dimensional cone trajectory with chemical shift-based fat saturation fat suppression.

signal of epimysium in 3D UTE. An epimysium contains not only collagen fibers but also fat cells and capillaries which has long T2 values, so it does not seem to show as strong a high signal intensity in 3D UTE as deep peripheral fascia (24). The weak high signal in zone 2 may not fully reflect the tissue's short T2 value, possibly due to fat, partial volume effect, or off-resonance artifacts from non-Cartesian UTE acquisition (25).

In our study, we used dual-echo acquisition with echo subtraction for the short T2 contrast. However, the SNR and CNR are generally poor in subtraction images for both 3D UTE and 3D UTE FS, despite strong high signal intensity in deep peripheral fascia. The significant weakness of the dual-echo acquisition with echo subtraction was decreased SNR, residual long T2 signals, and magnetic susceptibility effects (26). Specific TEs can minimize errors (26). In our study, we used a 4.4 ms as a second TE to minimize the chemical shift effect, i.e., intravoxel signal cancellation of water and fat, as these elements come into phase around 4.4 ms (26). A shorter second TE was unattainable due to the limited performance of the gradient hardware. In dual echo UTE-gradient echo imaging, the minimum echo spacing is contingent on the duration of the preceding readout gradient and rewinder, which in turn depends on spatial resolution (i.e., voxel size), readout bandwidth, and gradient slew rate. According to prior study (27), the T2* value of the Achilles tendon is reported to be approximately 0.74±0.11, and its signal completely decays around 4 ms. Given that deep peripheral fascia and epimysium are connective tissues composed of collagen

bundles, similar to the Achilles tendon, it was hypothesized that their short T2* values would be similar. Consequently, a nominal TE of 0.032 ms and a long echo subtraction of 4.4 ms were deemed suitable for the selective detection of these structures' signals. However, chemically shifted lipid signals can still result in residual signals due to their variable nature, making accurate subtraction difficult (26).

Our study had several limitations. First, partial volume artifacts may have significantly influenced the SNR and CNR measurements in our study. The voxel size of the 3D UTE in our study was 0.5 mm × 0.5 mm × 3 mm, which is greater than the 0.1 mm thickness of the epimysium as observed in the histologic sections. Consequently, it is highly susceptible to inaccurate measurements due to the incorporation of adjacent tissue signals. Anatomical structures that are targets of 3D UTE, such as calcified cartilage layers, aponeuroses, tendons, and ligaments, often only measure a few millimeters in size. Therefore, it is essential to overcome partial volume artifacts for accurate evaluation of these structures. Technological advancements are needed to allow for the imaging of thinner sections, larger matrix sizes, or isotropic imaging within a clinically acceptable scan duration. The use of advanced accelerated UTE imaging techniques, which leverage compressed sensing or deep learning-based methodologies, could provide a breakthrough to achieving higher spatial resolutions within a clinically feasible scan time (28,29). Second, we used the chemical shift-based fat suppression to suppress fat signal adjacent to the deep peripheral fascia and epimysium. However, the chemical shift-based fat saturation is not well-suited for short T2 imaging as we mentioned above. FS for UTE imaging using a soft-hard composite RF pulse (23), long T2 suppression RF pulse (30), or the inversion recovery preparations (15,31) are being studied, but more research is needed to determine their clinical applicability. Third, the chemical shift-based FS is even insufficient because of the variable frequency of fat tissue and due to field inhomogeneity in 3D UTE and may not eliminate chemical shift artifacts as the result of the Experiment No. 1 demonstrated (23). Unfortunately, our MR system did not have higher-order shimming, which could potentially improve FS using the fat-sat pulse. Although, we believe the performance of FS was reasonable for the purpose of our study investigating morphological imaging. Fourth, the dual echo acquisition and echo subtraction technique is inaccurate method for suppression of long T2 signal and makes image degradation significant as we described above (26,32,33). Fifth, in the second experiment, we did not align the interval of the histological sections with that of the 3D UTE. Despite the interval of the histological sections being 6 mm—a multiple of the MRI interval which was 3 mm—this discrepancy is not conducive to an accurate MRI-histology correlation. Sixth, the 3D UTE signal and artifact of the tissue boundary can be affected by the parameters, coil, and MR scanner. Seventh, the small number of porcine lower legs did not allow statistical analysis to be performed. Eighth, our study did not include clinical cases with pathology of the deep peripheral fascia and epimysium; therefore, the diagnostic value of 3D UTE remains unclear. However, given that accurate validation of the signal of the deep peripheral fascia and epimysium should precede clinical studies, our study provides the basis for further clinical research.

Conclusions

In conclusion, 3D UTE and 3D UTE FS can be used to visualize the deep peripheral fascia with high signal intensity and contrast but is insufficient to show signal intensity in the epimysium.

Acknowledgments

We would like to thank the applicators and scientists at GE HealthCare (Korea) for their help in installing and setting up the 3D UTE.
Funding: None.

Footnote

Conflicts of Interest: All authors have completed the ICMJE uniform disclosure form (available at https://qims.amegroups.com/article/view/10.21037/qims-23-687/coif). The authors have no conflicts of interest to declare.

Ethical Statement: The authors are accountable for all aspects of the work in ensuring that questions related to the accuracy or integrity of any part of the work are appropriately investigated and resolved. The present study comprised two sets of experiments, ethical approval was exempted by the Institutional Review Board of Inha University Hospital due to the use of cadaveric animal specimen.

References

1. Gatt A, Agarwal S, Zito PM. Anatomy, Fascia Layers. Treasure Island, FL, USA: StatPearls Publishing; 2023.
2. Kirchgesner T, Demondion X, Stoenoiu M, Durez P, Nzeusseu Toukap A, Houssiau F, Galant C, Acid S, Lecouvet F, Malghem J, Vande Berg B. Fasciae of the musculoskeletal system: normal anatomy and MR patterns of involvement in autoimmune diseases. Insights Imaging 2018;9:761-71.
3. Stecco C, Porzionato A, Lancerotto L, Stecco A, Macchi V, Day JA, De Caro R. Histological study of the deep fasciae of the limbs. J Bodyw Mov Ther 2008;12:225-30.
4. Turrina A, Martínez-González MA, Stecco C. The muscular force transmission system: role of the intramuscular connective tissue. J Bodyw Mov Ther 2013;17:95-102.
5. Benjamin M. The fascia of the limbs and back--a review. J Anat 2009;214:1-18.
6. Stecco C, Macchi V, Porzionato A, Duparc F, De Caro R. The fascia: the forgotten structure. Ital J Anat Embryol 2011;116:127-38.
7. Tyler DJ, Robson MD, Henkelman RM, Young IR, Bydder GM. Magnetic resonance imaging with ultrashort TE (UTE) PULSE sequences: technical considerations. J Magn Reson Imaging 2007;25:279-89.
8. Bae WC, Dwek JR, Znamirowski R, Statum SM, Hermida JC, D'Lima DD, Sah RL, Du J, Chung CB. Ultrashort echo time MR imaging of osteochondral junction of the knee at 3 T: identification of anatomic structures contributing to signal intensity. Radiology 2010;254:837-45.
9. Bae WC, Statum S, Zhang Z, Yamaguchi T, Wolfson T, Gamst AC, Du J, Bydder GM, Masuda K, Chung CB. Morphology of the cartilaginous endplates in human intervertebral disks with ultrashort echo time MR imaging. Radiology 2013;266:564-74.
10. Hwang D, Kim S, Abeydeera NA, Statum S, Masuda K, Chung CB, Siriwanarangsun P, Bae WC. Quantitative magnetic resonance imaging of the lumbar intervertebral discs. Quant Imaging Med Surg 2016;6:744-55.
11. Wilms LM, Radke KL, Latz D, Thiel TA, Frenken M, Kamp B, Filler TJ, Nagel AM, Müller-Lutz A, Abrar DB, Nebelung S. UTE-T2* versus conventional T2* mapping to assess posterior cruciate ligament ultrastructure and integrity-an in-situ study. Quant Imaging Med Surg 2022;12:4190-201.
12. Omoumi P, Bae WC, Du J, Diaz E, Statum S, Bydder GM, Chung CB. Meniscal calcifications: morphologic and quantitative evaluation by using 2D inversion-recovery ultrashort echo time and 3D ultrashort echo time 3.0-T MR imaging techniques--feasibility study. Radiology 2012;264:260-8.
13. Lu X, Jang H, Ma Y, Jerban S, Chang EY, Du J. Ultrashort Echo Time Quantitative Susceptibility Mapping (UTE-QSM) of Highly Concentrated Magnetic Nanoparticles: A Comparison Study about Different Sampling Strategies. Molecules 2019;24:1143.
14. Wan L, Zhao W, Ma Y, Jerban S, Searleman AC, Carl M, Chang EY, Tang G, Du J. Fast quantitative 3D ultrashort echo time MRI of cortical bone using extended cones sampling. Magn Reson Med 2019;82:225-36.
15. Carl M, Bydder GM, Du J. UTE imaging with simultaneous water and fat signal suppression using a time-efficient multispoke inversion recovery pulse sequence. Magn Reson Med 2016;76:577-82.
16. Ma YJ, Carl M, Shao H, Tadros AS, Chang EY, Du J. Three-dimensional ultrashort echo time cones T(1ρ) (3D UTE-cones-T(1ρ)) imaging. NMR Biomed 2017;30:10.1002/nbm.3709.
17. Landis JR, Koch GG. The measurement of observer agreement for categorical data. Biometrics 1977;33:159-74.
18. Bydder GM, Chung CB. Magnetic resonance imaging of short T2 relaxation components in the musculoskeletal system. Skeletal Radiol 2009;38:201-5.
19. Bydder M, Carl M, Bydder GM, et al. MRI chemical shift artifact produced by center-out radial sampling of k-space: a potential pitfall in clinical diagnosis. Quant Imaging Med Surg 2021;11:3677-83.
20. Holmes JE, Bydder GM. MR imaging with ultrashort TE (UTE) pulse sequences: Basic principles. Radiography 2005;11:163-74.
21. Jang H, Carl M, Ma Y, Jerban S, Guo T, Zhao W, Chang EY, Du J. Fat suppression for ultrashort echo time imaging using a single-point Dixon method. NMR Biomed 2019;32:e4069.
22. Henkelman RM, Stanisz GJ, Graham SJ. Magnetization transfer in MRI: a review. NMR Biomed 2001;14:57-64.

23. Ma YJ, Jerban S, Jang H, Chang EY, Du J. Fat suppression for ultrashort echo time imaging using a novel soft-hard composite radiofrequency pulse. Magn Reson Med 2019;82:2178-87.
24. Maynard RL, Downes N. Chapter 6 - The Musculature of the Rat. Anatomy and Histology of the Laboratory Rat in Toxicology and Biomedical Research. Academic Press; 2019:57-76.
25. Chang EY, Du J, Chung CB. UTE imaging in the musculoskeletal system. J Magn Reson Imaging 2015;41:870-83.
26. Du J, Bydder M, Takahashi AM, Carl M, Chung CB, Bydder GM. Short T2 contrast with three-dimensional ultrashort echo time imaging. Magn Reson Imaging 2011;29:470-82.
27. Chen B, Zhao Y, Cheng X, Ma Y, Chang EY, Kavanaugh A, Liu S, Du J. Three-dimensional ultrashort echo time cones (3D UTE-Cones) magnetic resonance imaging of entheses and tendons. Magn Reson Imaging 2018;49:4-9.
28. Athertya JS, Ma Y, Masoud Afsahi A, Lombardi AF, Moazamian D, Jerban S, Sedaghat S, Jang H. Accelerated Quantitative 3D UTE-Cones Imaging Using Compressed Sensing. Sensors (Basel) 2022;22:7459.
29. Byra M, Wu M, Zhang X, Jang H, Ma YJ, Chang EY, Shah S, Du J. Knee menisci segmentation and relaxometry of 3D ultrashort echo time cones MR imaging using attention U-Net with transfer learning. Magn Reson Med 2020;83:1109-22.
30. Larson PE, Gurney PT, Nayak K, Gold GE, Pauly JM, Nishimura DG. Designing long-T2 suppression pulses for ultrashort echo time imaging. Magn Reson Med 2006;56:94-103.
31. Ma YJ, Zhu Y, Lu X, Carl M, Chang EY, Du J. Short T(2) imaging using a 3D double adiabatic inversion recovery prepared ultrashort echo time cones (3D DIR-UTE-Cones) sequence. Magn Reson Med 2018;79:2555-63.
32. C A Araujo E, Azzabou N, Vignaud A, Guillot G, Carlier PG. Quantitative ultrashort TE imaging of the short-T(2) components in skeletal muscle using an extended echo-subtraction method. Magn Reson Med 2017;78:997-1008.
33. Wehrli FW, Ma J, Hopkins JA, Song HK. Measurement of R'2 in the presence of multiple spectral components using reference spectrum deconvolution. J Magn Reson 1998;131:61-8.

Cite this article as: Hwang K, Cha JG, Kim H, Jang H, Kim DJ, Lee S, Kim YJ. Ultrashort echo time pulse sequences for visualization of deep peripheral fasciae and epimysium in porcine models with histologic correlations. Quant Imaging Med Surg 2023;13(12):8447-8461. doi: 10.21037/qims-23-687

